THE JOURNAL OF BIOLOGICAL CHEMISTRY VOL. 290, NO. 48, pp. 28737–28745, November 27, 2015

Structural Mechanism of the Interaction of Alzheimer Disease Aβ Fibrils with the Non-steroidal Anti-inflammatory Drug (NSAID) Sulindac Sulfide*[S]

Received for publication, June 27, 2015, and in revised form, September 14, 2015 Published, JBC Papers in Press, September 28, 2015, DOI 10.1074/jbc.M115.675215

Elke Prade[‡], Heiko J. Bittner[§], Riddhiman Sarkar[‡], Juan Miguel Lopez del Amo[¶], Gerhard Althoff-Ospelt[‖], Gerd Multhaup[1], Peter W. Hildebrand[§], and Bernd Reif[‡ ‡‡2]**

From the [‡]Munich Center for Integrated Protein Science at Department Chemie, Technische Universität München, Lichtenbergstr. 4, 85747 Garching, Germany, [§]Molecular Modeling, Institute of Medical Physics and Biophysics, Universitätsmedizin Berlin, Charitéplatz 1, 10117 Berlin, Germany, [¶]CIC Energigune, Albert Einstein 48, 01510 Miñano, Álava, Spain, [‖]Bruker BioSpin, Silberstreifen 4, 76287 Rheinstetten, Germany, the [**]Department of Pharmacology and Therapeutics, McGill University, Montreal Quebec H3G 1Y6, Canada, and the [‡‡]Helmholtz-Zentrum München, Deutsches Forschungszentrum für Gesundheit und Umwelt, Ingolstädter Landtstr. 1, 85764 Neuherberg, Germany

Background: The mechanism of interaction between small molecules and amyloid-β fibrils is unknown.
Results: Molecular modeling on the basis of solid-state NMR reveals that sulindac sulfide intercalates between β-strands of amyloid-β fibrils.
Conclusion: Sulindac sulfide interacts with amyloid-β fibrils in a specific manner and binds to hydrophobic cavities in the core of the fibrils.
Significance: Unraveling how small molecules interfere with amyloidogenic deposits will assist structure-based drug design for neurodegenerative disorders.

Alzheimer disease is the most severe neurodegenerative disease worldwide. In the past years, a plethora of small molecules interfering with amyloid-β (Aβ) aggregation has been reported. However, their mode of interaction with amyloid fibers is not understood. Non-steroidal anti-inflammatory drugs (NSAIDs) are known γ-secretase modulators; they influence Aβ populations. It has been suggested that NSAIDs are pleiotrophic and can interact with more than one pathomechanism. Here we present a magic angle spinning solid-state NMR study demonstrating that the NSAID sulindac sulfide interacts specifically with Alzheimer disease Aβ fibrils. We find that sulindac sulfide does not induce drastic architectural changes in the fibrillar structure but intercalates between the two β-strands of the amyloid fibril and binds to hydrophobic cavities, which are found consistently in all analyzed structures. The characteristic Asp^{23}-Lys^{28} salt bridge is not affected upon interacting with sulindac sulfide. The primary binding site is located in the vicinity of residue Gly^{33}, a residue involved in Met^{35} oxidation. The results presented here will assist the search for pharmacologically active molecules that can potentially be employed as lead structures to guide the design of small molecules for the treatment of Alzheimer disease.

The self-assembly of amyloidogenic proteins into fibrils and oligomers plays a pivotal role in various diseases (1). The deposition of fibrils formed by the amyloid-β peptide (Aβ)[3] into plaques in brain tissue is a major pathological hallmark in the progression of neurodegeneration in Alzheimer disease. Aβ peptides are generated through sequential proteolytic cleavages of the amyloid precursor protein (APP) by the β- and γ-secretases (2, 3). This results in the production of Aβ peptides of differing lengths (4), mainly $Aβ_{1-40}$ and $Aβ_{1-42}$ (5), and shorter variants, such as $Aβ_{1-39}$ (6). Soluble oligomers formed by $Aβ_{1-42}$ represent the toxic species responsible for the decline in cognitive function associated with neurodegeneration (7). Several studies have demonstrated that small molecules can interfere with the solubility of amyloid proteins and are, therefore, potential drug candidates (8, 9). Chronic inflammation significantly enhances Alzheimer disease pathogenesis (10). Fibrillar β-amyloid deposits co-localize with numerous chronic inflammatory mediators and activated microglia in the brain (11). The relation to inflammation suggests that non-steroidal anti-inflammatory drugs (NSAIDs) might be beneficial for the treatment of Alzheimer disease. In fact, epidemiological studies demonstrate a link between the use of anti-inflammatory drugs and the prevalence of Alzheimer disease (12). This work aims to investigate the interaction mechanism of the NSAID sulindac sulfide (Fig. 1*a*) with Alzheimer peptide Aβ fibrils. In addition to sulindac sulfide (13), NSAIDs, including ibuprofen, indomethacin (13), and flurbiprofen (14), have been identified as

* This work was supported by the Center for Integrated Protein Science Munich, the Helmholtz-Gemeinschaft, and the Deutsche Forschungsgemeinschaft (Grant Re1435). This work was also supported by Canadian Institute of Health Research Grant MOP-133411 and infrastructure (to G. M.). The authors declare that they have no conflicts of interest with the contents of this article.
[S] This article contains supplemental Results, Figures S1–S8, Tables S1–S3, and References.
[1] Holder of a Canada Research Chair in Molecular Pharmacology and supported by CFI grants.
[2] To whom correspondence should be addressed: E-mail: reif@tum.de.

[3] The abbreviations used are: Aβ, amyloid-β; APP, amyloid precursor protein; NSAID, non-steroidal anti-inflammatory drug; DMSO, dimethyl sulfoxide; MAS, magic angle spinning; TEDOR, transferred echo double resonance; REDOR, rotational echo double resonance; TEM, transmission electron microscopy.

γ-secretase modulators. γ-Secretase modulators interfere with APP processing and modify the relative $A\beta_{1-42}$ population. In particular, sulindac sulfide decreases the relative amount of the amyloid-prone $A\beta_{1-42}$, whereas the production of shorter, less amyloidogenic Aβ peptides is increased (13–16).

Solution-state NMR structures of the APP-TM (transmembrane) dimer have been solved for the wild-type (17) and a familial mutant (18). NMR and EPR experiments have revealed a potential cholesterol-binding site within the C-terminal Cys^{99} sequence and highlight the significance of the G*XXX*G segments for binding (19). It has been suggested that NSAIDs can interact with lipids to form phospholipid complexes (20–22). This may provide a general mechanism for the interaction of APP with small molecules. Reports on the interaction between sulindac sulfide and the APP transmembrane sequence are, however, contradictory. Sulindac sulfide, among other γ-secretase modulators, binds to the APP transmembrane sequence of the Cys^{99} motif (23) and to Cys^{100} dimers in the presence of SDS micelles (24). Bacterial reporter assays show that γ-secretase modulators, including sulindac sulfide, bind to the G*XXX*G dimerization motif and, thereby, attenuate the dimerization of the APP transmembrane sequence (25), a process necessary for proteolytic cleavage (26). However, colloidal aggregation of sulindac sulfide in aqueous solutions can potentially induce nonspecific binding (27, 28). Contradicting data have been reported for the influence of sulindac sulfide on the Aβ peptide itself (29, 30).

So far, it is not understood how sulindac sulfide interacts with amyloids. NMR is a suitable technique to study Aβ-ligand interactions for various Aβ aggregation states (31). Solution-state NMR can be employed to study interactions of Aβ monomers and small molecule (32) or peptide inhibitors (33), nanoparticles (34), and various others. Besides monomers and fibrils, oligomeric intermediates formed by Aβ in solution constitute potential drug targets (35, 36). However, oligomeric intermediates and insoluble fibrils are not detectable by solution-state NMR because their lines are broadened beyond detection. Solid-state NMR spectroscopy is a powerful tool that allows the study of Aβ-small molecule interactions at atomic resolution. In the past, this technique has been applied successfully for the characterization of the interaction between Aβ and the polyphenol epigallocatechin gallate (37), curcumin (38, 39), and catechol-type flavonoids (40) and to study the interface of Congo red and amyloids formed by the prion domain of the HET-s protein (41). In this work, we investigate the interaction between sulindac sulfide and Aβ fibrils using solid-state NMR spectroscopy. On the basis of the gathered NMR data, we employ docking to derive a model for the intercalation of sulindac sulfide with Aβ fibrils.

Experimental Procedures

Aβ Expression and Purification and Sample Preparation—The uniformly ^{15}N or ^{15}N-^{13}C-labeled $A\beta_{1-40}$ peptide was recombinantly expressed in *Escherichia coli* inclusion bodies and purified via reverse-phase chromatography as described previously (42). The construct contains an N-terminal methionine but shows the same biochemical properties as the wild-type peptide (43). To obtain monomeric Aβ in solution, the lyophilized peptide was initially dissolved in 10 mM NaOH, sonicated for 10 min in an ultrasonic bath, and centrifuged for 10 min at 14,800 rpm to remove potential nucleation seeds. The solution was then diluted in 2× buffer (100 mM sodium phosphate and 100 mM NaCl buffer (pH 7.3)) to yield the respective Aβ concentration.

Preparation of NSAIDs—Stock solutions of sulindac sulfide were prepared in dimethyl-sulfoxide (DMSO), and the respective amount of NSAID stock was added to Aβ. The final concentration of DMSO in aqueous solutions was 1%.

Solid-state NMR Sample Preparation—Aβ fibrils were obtained according to a protocol described previously (44). Briefly, monomeric Aβ at a concentration of 50 μM was seeded with sonicated fibrils (10% w/w) and incubated under agitation until the completion of fibrillation. This step was repeated for 11 generations. For solid-state NMR measurements, the last generation was allowed to fibrilize for 2 days before sulindac sulfide was added to the sample. Approximately 10 mg of Aβ fibrils was incubated with a 5-fold molar excess of sulindac sulfide (250 μM, 1% DMSO). After mixing, the sample was kept quiescent for 1 h at room temperature. As a reference, Aβ fibrils were incubated under the same conditions with 1% DMSO. The sulindac sulfide-incubated fibrils were sedimented into a 3.2-mm rotor. The reference fibrils were packed into a 4.0-mm rotor.

Solid-state NMR Measurements—^{13}C-detected assignment experiments were carried out using a Bruker Avance wide-bore spectrometer operating at a ^{1}H Larmor frequency of 700 MHz (16.5 tesla). The spectrometer was equipped with a triple-resonance MAS probe (^{1}H, ^{13}C, ^{15}N). All measurements were recorded at a MAS rotation frequency of 17 kHz for 3.2-mm rotors or 13 kHz for 4.0-mm rotors and a temperature of 12 °C. In all experiments, ^{1}H-^{13}C magnetization transfer was achieved through cross-polarization. Two-dimensional spectra were recorded using proton-driven spin diffusion (45, 46) for ^{13}C-^{13}C magnetization transfer with a mixing time of 200 ms or transferred echo double-resonance (TEDOR) (47, 48) for ^{13}C-^{15}N magnetization transfer. The three-dimensional NCACX and NCOCX (49) experiments were recorded employing TEDOR for ^{13}C-^{15}N magnetization transfer and dipolar assisted rotational resonance (50) for ^{13}C-^{13}C mixing.

To identify ^{13}C atoms in Aβ that are located in the vicinity of the ^{19}F atom of sulindac sulfide, we recorded ^{13}C-^{19}F rotational echo double resonance (REDOR) experiments (supplemental Fig. S8 *a*) (51). These were recorded on a Bruker Avance III wide-bore spectrometer operating at a ^{1}H Larmor frequency of 600 MHz (14 tesla). The spectrometer was equipped with a triple-resonance cross-polarization MAS probe (^{1}H, ^{13}C, ^{19}F). All measurements were recorded at a MAS rotation frequency of 14.6 kHz and a temperature of 12 °C. In the REDOR experiments, ^{13}C-^{19}F dipolar dephasing was preceded by a ^{13}C-^{13}C proton-driven spin diffusion mixing step. REDOR dephasing times were set to 1.1, 2.2, and 4.4 ms. REDOR spectra recorded with and without dephasing pulses were subtracted to identify fluorine-coupled carbons. In Fig. 2*a*, REDOR spectra are represented in one-dimensional mode. No ^{13}C-^{13}C cross peaks could be observed in the three-dimensional REDOR experiments because the sensitivity was too low. To detect the characteristic

salt bridge between the carboxyl of Asp^{23} and the amine of Lys^{28} of mature Aβ fibrils, TEDOR experiments (supplemental Fig. S8 *b*) were carried out on the basis of the pulse sequence described by Jaroniec *et al.* (52). All spectra were recorded on a Bruker Avance III narrow-bore spectrometer operating at a ^{1}H Larmor frequency of 750 MHz (17.63 tesla) equipped with a triple-resonance MAS probe (^{1}H, ^{13}C, ^{15}N) at a MAS rotation frequency of 11 kHz and 4 °C. In the experiment, the TEDOR mixing time was set to 7.27 and 15.72 ms.

Transmission Electron Microscopy (TEM)—Images were recorded on an EM 900 from Carl Zeiss SMT. Samples were stained with 4% uranyl acetate solution on formvar/carbon-coated grids.

Molecular Modeling—The 2-fold symmetric (PDB code 2LMN) (53) and the 3-fold symmetric (PDB code 2LMP) (54) $A\beta_{1-40}$ fibril NMR structural models were employed in molecular modeling studies. To identify internal cavities, each model of the Aβ fibril was analyzed separately. For the calculation of internal cavities, van der Waals volumes were derived using the Voronoi cell method (55, 56). Atomic volumes are calculated on the basis of the allocation of space among atoms using hyperbolic surfaces (applying a cubic lattice of 0.1-Å grid width) and applying the ProtOr (57) atom radius set for protein atoms that were determined analytically from reference structures. Internal cavities are determined analytically from each model structure by a Delaunay triangulation (58). An internal cavity is defined as the buried space within a structure that is big enough to accommodate at least a 1.4-Å radius water-sized probe. The size of a cavity is estimated from the average distance of the cavity center to the neighboring atoms and depicted by the radius of a sphere. The polarity of the cavities is assessed with the program DOWSER (59), which calculates potential positions for water not resolved by the original structure determination approach. This program assesses the hydrophilicity of protein cavities by determining the interaction energy between a water molecule and its surrounding atoms. Water molecules with interaction energies of less than −10 kcal/mol are considered "low-energy water molecules" and selected for output. Internal cavities harboring such an internal water molecule are denoted as polar (blue) and the remaining cavities as hydrophobic (gray) (Fig. 3 and supplemental Figs. S4 and S5).

For induced fit docking (60, 61), the region between the two most hydrophobic cavity clusters (termed #1-#5) near Ile^{32} (#2) and Val^{36} (#3) from the first NMR model was targeted. Docking was performed using the Schrödinger Maestro suite (62) following a standard protocol. Subsequently, a grid with auto-assigned box size was generated. The resulting box is centered near Leu^{34} for the 3-fold symmetric structure and Ile^{32} and Val^{36} for the 2-fold symmetric structure. Induced fit docking was done with the program Glide with single precision and with no constraints applied (63). To simulate receptor flexibility, side chain orientations were optimized to take into account ligand binding. At last, a Glide redocking was applied for the refined structure. Docking poses are ranked and filtered by means of the Glide score. This score assesses the binding probability and accounts for steric clashes, van der Waals and coulomb energy, lipophilicity, H-bonding, and bond rotation ability, among others. Only the energetically most favorable docking poses (with theoretical energies <30 kcal/mol higher than the best pose) are considered for further analysis.

Results

To probe the interaction between Aβ fibrils and sulindac sulfide (Fig. 1*a*), we titrated sulindac sulfide to preformed fibrils. Fibrillar Aβ is observed by TEM in the presence of the NSAID (Fig. 1*b*). The resulting ^{13}C-^{15}N (Fig. 1*c*) and ^{13}C-^{13}C (supplemental Fig. S1) correlation spectra show well dispersed peaks. The three-dimensional NCACX and NCOCX experiments allowed sequential assignment of resonances for residues Gln^{15}-Val^{40} for both samples (representative strip plots are shown in supplemental Fig. S2; all assigned resonances are listed in supplemental Table S1). We detected only one set of resonances for both samples, indicating that the fibrils exist in one conformation.

Sulindac sulfide has no significant effect on the fibrillar structure of Aβ because the spectra of both samples are relatively similar (Fig. 1*c* and supplemental Fig. S1). However, small but defined chemical shift perturbations (CSPs) are observed in the presence of sulindac sulfide, indicating specific interactions of the NSAID with the fibrils. This is remarkable because a non-quantitative and nonspecific binding of sulindac sulfide to Aβ fibrils would result in peak-splitting and line-broadening. Fig. 1*d* shows CSPs, Δδ (parts per million), upon addition of sulindac sulfide. We observe changes in chemical shift in particular for side chain resonances of Lys^{16}, Val^{18}-Cβ, Phe^{19}-Cβ, Phe^{20}-Cβ, Asn^{27}-Cγ, and Met^{35}-Cβ as well as for the backbone resonances of Phe^{19}, Phe^{20}, Ala^{21} and Gly^{33}. CSPs reflect ligand binding but could as well be a consequence of local or global structural rearrangements. To unambiguously probe ligand binding, we recorded ^{13}C-^{19}F REDOR experiments employing the NMR-active properties of the ^{19}F atom of sulindac sulfide. In general, only aliphatic resonances of Aβ could be detected. For comparison, a one-dimensional ^{13}C spectrum containing assignments for all aliphatic resonances is represented (Fig. 2*a*). The strongest dephasing effects are observed for the Cγ resonances of Val^{18} or Val^{39}. However, because of spectral overlap, these two peaks cannot be discriminated. Smaller signal attenuations are observed for Cγ of Val^{24} and Val^{36}, Cβs of Ala^{21} or Ala^{30} (overlap) as well as for Cγ2 and Cδ1 of Ile^{32} at longer mixing times. These resonances exhibit the most severe dephasing effects. The respective residues must therefore be located close to the fluorine atom of sulindac sulfide.

To gain further information on the potential effects of sulindac sulfide on the Aβ fibril structure, we investigated the effect on the salt bridge, which is typically formed between the side chains of residues Asp^{23} and Lys^{28} (53, 54). From sequential assignments, the chemical shift of the carboxylic group of Asp^{23} in the presence of sulindac sulfide was assigned to 177.8 ppm and to 178.0 ppm for the reference fibrils. On the basis of one-dimensional ^{15}N spectra, the chemical shift of Lys^{28}-Nζ was found to be 33.9 ppm and 34.3 ppm for the two preparations, respectively. In both samples, a cross-peak between Lys^{28}-Nζ and Asp^{23}-Cγ was detected, implying the presence of a salt bridge in both cases (Fig. 2*b*).

In the following, the CSPs in the two-dimensional ^{13}C-^{13}C proton-driven spin diffusion and ^{13}C-^{15}N TEDOR as well as the

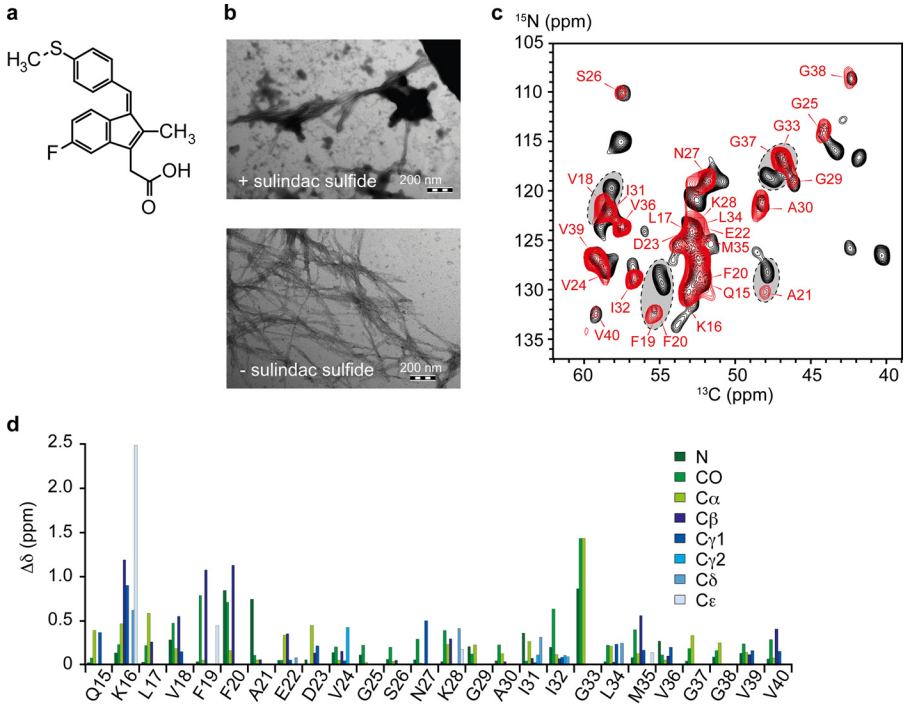

FIGURE 1. **The influence of sulindac sulfide on Aβ.** *a*, chemical structure of the NSAID sulindac sulfide. *b*, TEM images of 50 μM Aβ fibrils in the absence (*bottom panel*) and presence (*top panel*) of a 5-fold molar excess of sulindac sulfide. The fibrillar character is maintained, and deposits of sulindac sulfide can be observed. *Scale bar* = 200 nm. *c*, two-dimensional ^{13}C-^{15}N TEDOR spectra of Aβ amyloid fibrils incubated in the presence of a 5-fold molar excess of sulindac sulfide and 1% DMSO (*red*) and Aβ fibrils incubated with 1% DMSO (*black*) as a control. Corresponding ^{13}C-^{13}C correlation spectra are shown in supplemental Fig. S1. The obtained ^{13}C line widths are in the order of 120–200 Hz (data not shown). Sequential assignments are obtained from three-dimensional NCACX and NCOCX experiments. *Arrows* indicate residues that experience large chemical shift changes. *d*, CSPs induced by sulindac sulfide on the NMR chemical shifts of Aβ fibrils. Differences in chemical shifts (Δδ *(ppm)*) were calculated for ^{13}C and ^{15}N resonances according to $\Delta\delta_C = [(\delta C_{sul} - \delta C_{ref})^2]^{1/2}$ and $\Delta\delta_N = [(2/5 \times (\delta N_{sul} - \delta N_{ref}))^2]^{1/2}$, respectively.

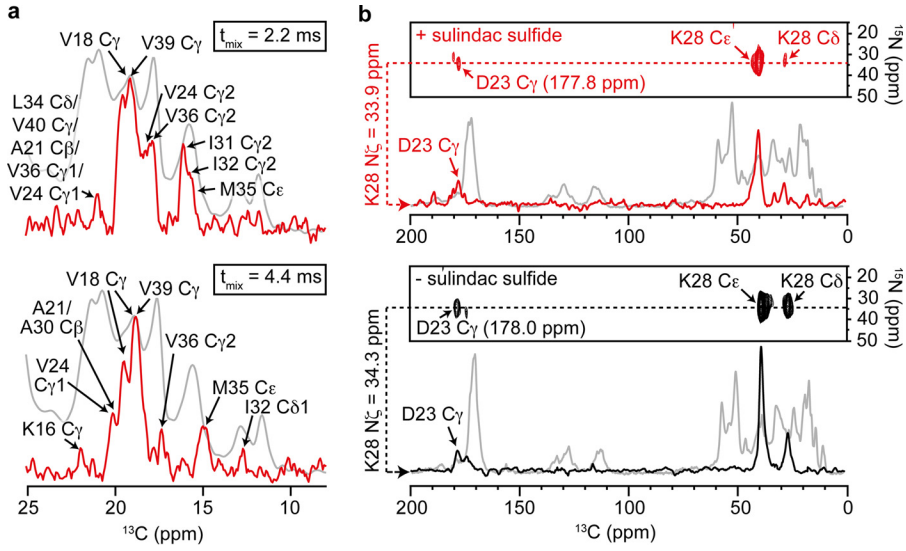

FIGURE 2. **^{13}C-^{19}F REDOR and ^{13}C-^{15}N TEDOR NMR experiments.** *a*, ^{13}C-^{19}F REDOR NMR experiments recorded to observe dephasing of Aβ ^{13}C nuclei in close proximity to the ^{19}F atom of sulindac sulfide. Experiments were run with mixing times of 1.1 (data not shown), 2.2, and 4.4 ms. A list of all ^{13}C-^{19}F contacts observed can be found in supplemental Table S2. Recoupled and reference spectra were subtracted to identify affected ^{13}C resonances (*red*). For reference, a one-dimensional ^{13}C experiment without ^{19}F recoupling, including all aliphatic resonances, is shown (*gray*). *b*, analysis of the salt bridge involving residues Asp^{23} and Lys^{28}. ^{13}C-^{15}N TEDOR spectra show cross-peaks between Lys^{28}-Nζ and Asp^{23}-Cγ in the presence (*red*) and absence of sulindac sulfide (*black*). A TEDOR mixing time of 15.72 ms is employed. One-dimensional traces extracted at the Nζ chemical shifts are superimposed with the one-dimensional ^{13}C reference spectra of the respective sample (*gray*).

^{13}C-^{19}F REDOR contacts were used as restraints to derive a model for sulindac sulfide in complex with $A\beta_{1-40}$ fibrils. We used both a 2-fold (53) and 3-fold symmetric (54) $A\beta_{1-40}$ fibril NMR structure as reference structures for modeling and docking experiments because they show the highest correlation with our chemical shifts (supplemental Fig. S3) compared with all structures and models analyzed (44, 53, 54, 64–68). The NMR structures contained 10 models each. The architecture of the $A\beta_{1-40}$ fibrils obviously differs comparing the 2-fold and 3-fold-symmetric structures. In each structure, Aβ adopts a

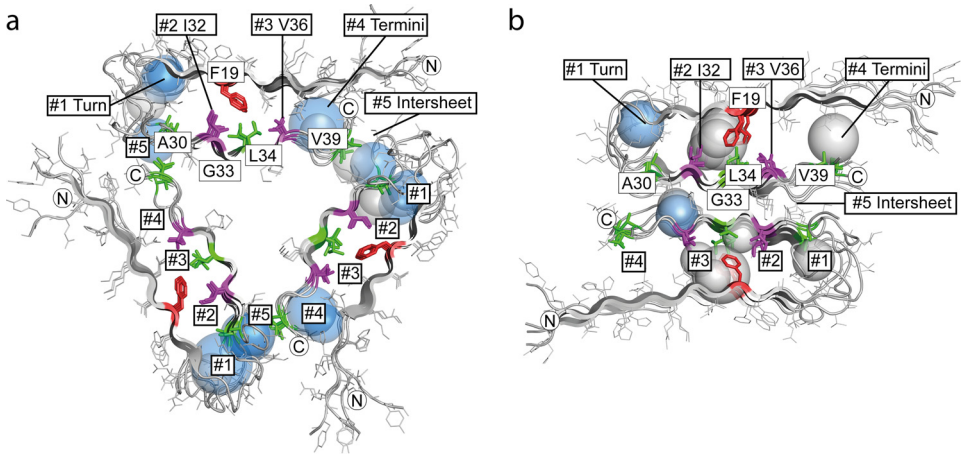

FIGURE 3. **Packing analysis of Aβ structures.** *a* and *b*, distribution of internal cavities in 3-fold symmetric $A\beta_{1-40}$ fibrils (PDB code 2LMP, *model 1*) (54) (*a*) and 2-fold symmetric $A\beta_{1-40}$ fibrils (PDB code 2LMN, *model 1*) (53) (*b*). Shown is a cross-section perpendicular to the fibril axis. Each cavity is depicted as a *sphere*. The radius of the sphere corresponds to the average distance from the cavity center to the Aβ van der Waals surface. Water-containing polar cavities are colored in *blue* and hydrophobic cavities in *gray*. The approximate position of cavity clusters #1 to #5 is indicated. The protein backbones are depicted as *schematics*, with side chains drawn as *lines*. Residues that are as close as ≤6 Å to the ^{19}F atom of sulindac sulfide are highlighted using *sticks*. Residues Ile^{32} and Val^{36}, which define cavity clusters, are represented in *purple*. Ala^{30}, Leu^{34}, and Val^{39} are shown in *green*. Phe^{19} is colored *red*. Termini are marked with *N* or *C*.

β-strand—turn—β-strand fold. Fibrils are stabilized by hydrogen bonds connecting individual β-strands along the fibril axis. The 3-fold symmetric fibril structure contains three stacks of Aβ molecules in a triangular form. The 2-fold symmetric fibril structure is built from two antiparallel stacks of Aβ molecules. To detect potential binding sites for the hydrophobic sulindac sulfide, we performed a packing density analysis for each Aβ structure. In fact, all models revealed large packing defects. On average, we found eight cavities per stack of four Aβ molecules in both structures (supplemental Figs. S4 and S5), clustering in five different regions within one stack (clusters #1-#5) (Fig. 3). To dissect polar from unpolar cavities, we applied the tool DOWSER (59) to calculate positions of internal water molecules that are not resolved in the NMR structures. We found that the most hydrophobic cavities in each structure clustered in the rigid core region, with calculated water occupancies of <10% in cluster #2 and <30% in cluster #3 that are located on both sides of Phe-19 (supplemental Table S3). The 3-fold symmetric structure seemed to be more tightly packed around clusters #2 and #3, featuring fewer cavities in comparison with the 2-fold symmetric structure. At the same time, other clusters in the 3-fold symmetric structure seemed to contain a larger numbers of cavities. Clusters of polar cavities were found in the flexible turn region between residues Glu^{22} and Ile^{31} (cluster #1) and toward the termini of the peptide sequence (cluster #4). The two structures differed in their interface architecture between the termini to the adjacent loop region. Although, in the 3-fold symmetric structure, cavities of cluster #4 were stabilized through interactions with the loop, in the 2-fold symmetric structure, fewer polar cavities were found because the structure opened and cavities could become exposed. Cluster #5 (around M35) with polar cavities was located at the intersheet/contact region between termini and the loop region (3-fold symmetric structure) or at the interface of the antiparallel β-sheets (2-fold symmetric structure). In the intersheet region, where the contact interface between 3-fold and 2-fold symmetric structure was apparently different, the amount of cavities per stack (of four Aβ molecules) and their polarity did not differ. The amount of cavities and the respective water contents per cluster #1-#5 are shown in supplemental Table S3.

Clusters #2 and #3 contain large hydrophobic cavities, which could, in principle, bury a sulindac sulfide molecule. The exact size of the individual cavities depends on the rotameric state of Phe^{19}. The 3-fold symmetric and the 2-fold symmetric structures differ slightly in the position of Phe^{19} with respect to the registry of the second β-sheet containing residues Ile^{32} to Val^{36} (supplemental Fig. S6). In the 3-fold symmetric structure, Phe^{19} is oriented more toward Ile^{32}, whereas, in the 2-fold symmetric structure, Phe^{19} is pointing toward Leu^{34} and is, therefore, located more central in the core region. Surprisingly, the size, polarity, and distribution of the detected cavities is very similar in all analyzed structural models even though there are slight differences between the two models.

To test whether the hydrophobic cavities in clusters #2 and #3 are indeed suitable binding sites for sulindac sulfide, we applied an induced fit docking approach where the sulindac sulfide and side chains of Aβ were kept flexible. The size and accessibility of these cavities depends on the rotameric state of Phe^{19}. In fact, docking into cluster #3 of the 3-fold symmetric structure allows identification of two scenarios that fit to the distance restraints obtained from the NMR analysis. In particular, we find that the distance of the sulindac sulfide ^{19}F atom to the methyl groups of Ile^{32}, Leu^{34}, or Val^{36} is smaller than 6 Å. In pose 1, sulindac sulfide lies in the Gly^{33} groove and is orientated along the fibril axes, being close to Ile^{32} and Leu^{34}. The aromatic side chains of Phe^{19} are directed toward Ala^{30} (Fig. 4*a*, *top panel*). In pose 2, sulindac sulfide has rotated into a position with its conjugated ring system parallel to the β-sheets and orthogonal to Phe^{19} so that the ^{19}F atom approaches Leu^{34} and Val^{36}. (Fig. 4*a*, *bottom panel*). Both poses suggest an aromatic π stacking interaction between the conjugated ring system of sulindac sulfide and the Phe^{19} side chain. Similar interactions are obtained from docking to cluster #2 of the 2-fold symmetric structure (Fig. 4*b*). In pose 1, sulindac sulfide is orientated along the fibril axes, with its conjugated ring system parallel to Phe^{19}, analogous to pose 1 in the 3-fold symmetric structure. Again,

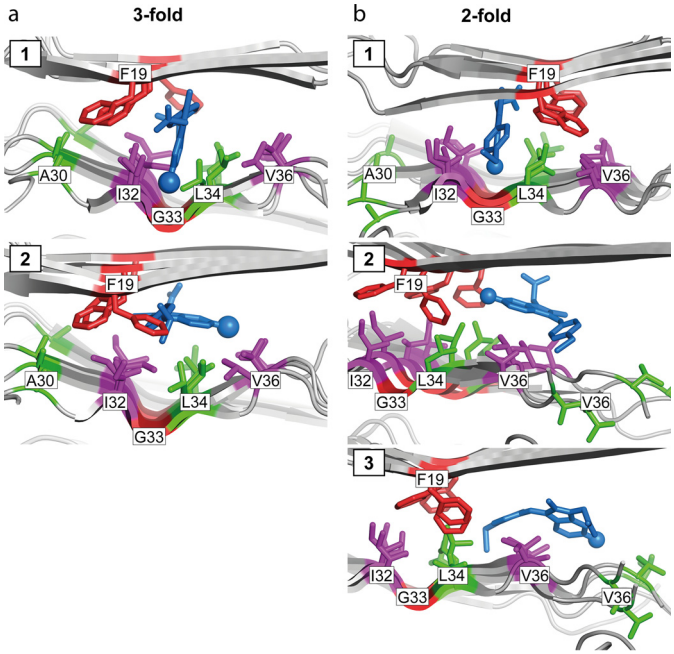

FIGURE 4. **Induced fit docking of sulindac sulfide to Aβ.** *a* and *b*, induced fit docking of sulindac sulfide to the hydrophobic cavity cluster #3 of the 3-fold symmetric $A\beta_{1-40}$ fibril structure (PDB code 2LMP, *model 1*, *poses 1* and *2*) (54) (*a*) and to the hydrophobic cavity clusters #2 and #3 of the 2-fold symmetric $A\beta_{1-40}$ structure (PDB code 2LMN, *model 1*; for cluster #2, *pose 1* and cluster #3, *poses 2* and *3*) (53) (*b*). Sulindac sulfide is depicted as *blue sticks* and the protein backbones as a *schematic*. Residues within 6 Å of the ^{19}F atom of sulindac sulfide are depicted as *sticks* in *purple* for the cavity cluster defining residues Ile^{32} and Val^{36} and in *green* for Ala^{30}, Leu^{34}, and Val^{39}. Phe^{19} and Gly^{33} are colored in *red*.

the ^{19}F atom is positioned in the Gly^{33} groove close to Ile^{32} and Leu^{34}. In contrast to the 3-fold symmetric structure, Phe^{19} is positioned here on the other side of sulindac sulfide, close to Leu^{34}, thereby shielding Val^{36} so that sulindac sulfide cannot change into a position to contact Val^{36} (Fig. 4*b*, *top panel*). An additional docking to cluster #3 yields poses 2 and 3, where the normal of the conjugated ring system of sulindac sulfide is orientated perpendicularly to the fibril axes. Thereby, sulindac sulfide extends into the terminal region (#4). The conjugated ring system is positioned parallel to the β-sheets and orthogonal to Phe^{19}. Sulindac sulfide is either orientated in a way that the ^{19}F atom faces Phe^{19}, Leu^{34}, and Val^{36} (Fig. 4*b*, *center panel*) or that the ^{19}F atom is oriented toward the fibril exterior, contacting Val^{36} and Val^{39} (Fig. 4*b*, *bottom panel*).

Discussion

Sulindac sulfide-incubated Aβ fibrils are highly similar to control fibrils, implying that sulindac sulfide has no significant effect on fibril structure. Both the NMR chemical shift patterns (Fig. 1*c* and supplemental Fig. S1) and the morphology in TEM images (Fig. 1*b*) are maintained. Analysis of ^{13}C chemical shifts predicts β-strands as the main secondary structural element in both fibril preparations (supplemental Fig. S7). In addition, chemical shift analysis by torsion angle likeliness obtained from shift and sequence similarities+ (TALOS+) (69) yields secondary structural propensities that predict the presence of two β-strands typically observed in specific regions within $A\beta_{1-40}$ fibrils (44, 53, 54, 67, 70) and oligomers (71, 72). Furthermore, we find, by TEDOR experiments, that the Asp^{23}-Lys^{28} salt bridge remains intact in the presence of sulindac sulfide (Fig. 2*b*). Even though the overall fibrillar character is maintained, we observe defined chemical shift changes, potentially indicating local conformational changes (Fig. 1*d*). Previous reports have stated that small molecules such as curcumin (39) are able to disrupt the characteristic salt bridge in $A\beta_{1-42}$ fibrils. Judging from EM data, curcumin has a more drastic effect on the general fibril architecture compared with sulindac sulfide because it destroys $A\beta_{1-42}$ fibrils (39). We note that only one set of resonances is observed for the sulindac sulfide-incubated Aβ fibrils. No resonance splitting is observed for cross-peaks. Rather, resonances move to new positions, indicating that each peptide in a fibril interacts specifically with one or more NSAID molecules.

Upon addition of sulindac sulfide, CSPs are observed in particular for hydrophobic residues such as Val^{18}, Phe^{19} and Phe^{20}, Gly^{33}, and Met^{35} but also for the polar side chain of Lys^{16}. The most dramatic CSPs are detected for Lys^{16} and Gly^{33} (Fig. 1*d*). ^{13}C-^{19}F REDOR experiments yield unambiguous distance restraints. The REDOR experiments show that sulindac sulfide binds in the vicinity of methyl groups of Val^{18} or Val^{39} as well as Ile^{31} and Ile^{32} Cγ2.

To identify trends and avoid bias, we use both the 2-fold symmetric (PDB code 2LMN) (53) and the 3-fold symmetric (PDB code 2LMP) (54) $A\beta_{1-40}$ fibrils as reference structures for modeling and docking experiments. The polymorphism of these structures may differ from the fibrils investigated in this study. However, they show the highest similarities of all three wild-type $A\beta_{1-40}$ fibril structures currently available (53, 54, 64). Within the two Aβ fibril structural ensembles, several hydrophobic cavities are detected that are large enough to potentially host a sulindac sulfide molecule. We did not find significant deviations in the distribution, size, and polarity of the cavities between the analyzed structural ensembles and models. Therefore, changes in fibril polymorphism do not significantly affect the distribution of hydrophobic patches in amyloid fibrils. We conclude that the two employed structures provide a suitable basis for docking experiments, which is also supported by experimental NMR data, although high-resolution structures of a better defined polymorph will allow more accurate docking in the future.

An induced fit docking reveals that the NSAID can interact with fibrils in three different ways, and all models fulfill the NMR restraints. The apparently ambiguous REDOR restraints suggest that more than one sulindac sulfide molecule might be involved in binding. In the docking poses that are in best agreement with the NMR restraints, sulindac sulfide intercalates between the two β-strands of the Aβ fibril, with the long axis of the molecule either parallel (Fig. 4, *a* and *b*, *pose 1*) or perpendicular (Fig. 4, *a*, *pose 2*, and *b*, *poses 2* and *3*) to the fibril axis. Therefore, residue Phe^{19} seems to play a crucial role in sulindac sulfide binding because its rotameric state has an influence on the size and shape of cavities in clusters #2 and #3. Furthermore, the aromatic side chain is involved in π stacking with the conjugated ring system of the NSAID.

Pose 1 of the docking approach suggests that sulindac sulfide fits into the groove formed by Gly^{33} (Fig. 4, *a* and *b*, *top panels*).

Therefore, the large CSPs may be attributed to Gly^{33} backbone atoms experiencing a change in chemical environment or even undergoing conformational changes to accommodate the NSAID. In theoretical studies, this glycine residue has been suggested to be involved in oxidation of $A\beta_{1-42}$ because of its close proximity to the side chain of Met^{35} (73, 74). Furthermore, Gly^{33} has been reported as the key amino acid for Aβ toxicity and to be responsible for driving Aβ into neurotoxic conformations (75). Both residues, Gly^{33} and Met^{35}, have been hypothesized to stabilize reactive oxygen species (76, 77). Sulindac sulfide might, therefore, act by binding to the hydrophobic pocket in the vicinity of Gly^{33}, and preventing oxidation of the Aβ peptide. Oxidation of $A\beta_{1-42}$ reduces fibril assembly and aggregation because of the increased polarity introduced by the methionine sulfoxide (78). In accordance, we find that the Aβ-sulindac sulfide complex exists in a stable fibrillar state.

CSPs for Lys^{16} may be explained by a recent docking study involving sulindac sulfide and Aβ fibrils that suggested that sulindac sulfide may bind weakly to a shallow, solvent-exposed pocket in the vicinity of Lys^{16} and Val^{18} and does not interfere with fibrillation (30). This binding mode may, in addition, account for the large REDOR signal detected for the overlapping resonances Val^{18}/Val^{39} Cγ (Fig. 2*a*). We cannot exclude docking of sulindac sulfide to the fibril surface because our REDOR and CSP data are also in agreement with the blind docking model proposed by Yesuvadian *et al.* (30).

Sulindac sulfide has been reported to form colloidal aggregates above a critical micelle concentration in solution (28). This phenomenon is commonly observed for hydrophobic compounds (79, 80). The size of small-molecule colloidal particles is typically on the order of 50–600 nm (28). These colloids bind unfolded proteins in a promiscuous manner (79, 80) and have been shown to lead to precipitation and inhibition of protein function (81–83). However, the effect of sulindac sulfide on Aβ fibril chemical shifts reported here indicates not a promiscuous but a specific interaction. Aggregates of the compound are observed in TEM images (Fig. 1*b*), implying the presence of colloids in solution. This is expected because the concentration used (250 μM) lies above the critical micelle concentration of 50–100 μM (28). To account for the experimental single set of resonances, we must assume that individual NSAID molecules dissociate from the colloidal complexes and interact specifically with Aβ fibrils.

Binding of sulindac sulfide in different cavities for different Aβ peptides would result in splitting of the resonances and line-broadening. We observe, however, narrow lines, indicating that the small molecule must either bind simultaneously to different cavities or exchange between these cavities. Relaxation experiments will be carried out in the future to differentiate between these two scenarios.

In conclusion, we suggest that the NSAID sulindac sulfide is able to interact with Aβ fibrils in a rather specific manner. We find that several cavities can accommodate a sulindac sulfide molecule. This is supported by defined CSPs and ^{13}C-^{19}F REDOR contacts. Sulindac sulfide does not induce drastic architectural changes to the non-toxic fibrillar structure, as indicated by NMR and EM. In addition, the characteristic Asp^{23}-Lys^{28} salt bridge and the length and positioning of the β-strands are not affected. Molecular modeling suggests that sulindac sulfide intercalates between the two β-strands at, presumably, more than one position. The presented data contribute to the elucidation of the mechanism by which small molecules bind insoluble amyloids. This understanding is crucial for the design of pharmacologically relevant molecules that interfere with Aβ species and that might, in the future, be employed for the treatment of Alzheimer disease.

Author Contributions—E. P. expressed and purified isotopically labelled peptide samples, designed and performed NMR experiments, and carried out the data analysis. R. S. implemented the solid-state NMR experiments. J. M. L. d. A. recorded the initial experiments and assisted with data analysis. G. A. O. carried out the fluorine REDOR experiments. G. M. performed biochemical experiments. H. J. B. and P. W. H. performed and analyzed the molecular modeling and docking. All authors discussed the results. B. R. and E. P. conceived the project and wrote the paper with input from all authors.

Acknowledgments—This work was performed in the framework of SFB-1035/Project-B07 and SFB740/Project-B6 (German Research Foundation). The computer time necessary for calculation of docking experiments was provided by Norddeutscher Verbund für Hoch- und Höchstleistungsrechner Project bec00085.

References

1. Bucciantini, M., Giannoni, E., Chiti, F., Baroni, F., Formigli, L., Zurdo, J., Taddei, N., Ramponi, G., Dobson, C. M., and Stefani, M. (2002) Inherent toxicity of aggregates implies a common mechanism for protein misfolding diseases. *Nature* **416,** 507–511
2. Haass, C. (2004) Take five: BACE and the γ-secretase quartet conduct Alzheimer's amyloid β-peptide generation. *EMBO J.* **23,** 483–488
3. Kang, J., Lemaire, H. G., Unterbeck, A., Salbaum, J. M., Masters, C. L., Grzeschik, K. H., Multhaup, G., Beyreuther, K., and Müller-Hill, B. (1987) The precursor of Alzheimer's disease amyloid A4 protein resembles a cell-surface receptor. *Nature* **325,** 733–736
4. Olsson, F., Schmidt, S., Althoff, V., Munter, L. M., Jin, S., Rosqvist, S., Lendahl, U., Multhaup, G., and Lundkvist, J. (2014) Characterization of intermediate steps in amyloid β (Aβ) production under near-native conditions. *J. Biol. Chem.* **289,** 1540–1550
5. Roher, A. E., Lowenson, J. D., Clarke, S., Woods, A. S., Cotter, R. J., Gowing, E., and Ball, M. J. (1993) β-Amyloid-(1–42) is a major component of cerebrovascular amyloid deposits: implications for the pathology of Alzheimer disease. *Proc. Natl. Acad. Sci. U.S.A.* **90,** 10836–10840
6. Prelli, F., Castaño, E., Glenner, G. G., and Frangione, B. (1988) Differences between vascular and plaque core amyloid in Alzheimer's disease. *J. Neurochem.* **51,** 648–651
7. Selkoe, D. J. (2008) Soluble oligomers of the amyloid β-protein impair synaptic plasticity and behavior. *Behav. Brain Res.* **192,** 106–113
8. Bieschke, J., Russ, J., Friedrich, R. P., Ehrnhoefer, D. E., Wobst, H., Neugebauer, K., and Wanker, E. E. (2010) EGCG remodels mature α-synuclein and amyloid-β fibrils and reduces cellular toxicity. *Proc. Natl. Acad. Sci. U.S.A.* **107,** 7710–7715
9. Bieschke, J., Herbst, M., Wiglenda, T., Friedrich, R. P., Boeddrich, A., Schiele, F., Kleckers, D., Lopez del Amo, J. M., Grüning, B. A., Wang, Q., Schmidt, M. R., Lurz, R., Anwyl, R., Schnoegl, S., Fändrich, M., Frank, R. F., Reif, B., Günther, S., Walsh, D. M., and Wanker, E. E. (2012) Small-molecule conversion of toxic oligomers to nontoxic β-sheet-rich amyloid fibrils. *Nat. Chem. Biol.* **8,** 93–101
10. Akiyama, H., Barger, S., Barnum, S., Bradt, B., Bauer, J., Cole, G. M., Cooper, N. R., Eikelenboom, P., Emmerling, M., Fiebich, B. L., Finch, C. E., Frautschy, S., Griffin, W. S., Hampel, H., Hull, M., Landreth, G., Lue, L., Mrak, R., Mackenzie, I. R., McGeer, P. L., O'Banion, M. K., Pachter, J.,

Pasinetti, G., Plata-Salaman, C., Rogers, J., Rydel, R., Shen, Y., Streit, W., Strohmeyer, R., Tooyoma, I., Van Muiswinkel, F. L., Veerhuis, R., Walker, D., Webster, S., Wegrzyniak, B., Wenk, G., and Wyss-Coray, T. (2000) Inflammation and Alzheimer's disease. *Neurobiol. Aging* **21,** 383–421

11. McGeer, P. L., and McGeer, E. G. (1995) The inflammatory response system of brain: implications for therapy of Alzheimer and other neurodegenerative diseases. *Brain Res. Brain Res. Rev.* **21,** 195–218
12. in t' Veld, B. A., Ruitenberg, A., Hofman, A., Launer, L. J., van Duijn, C. M., Stijnen, T., Breteler, M. M., and Stricker, B. H. (2001) Nonsteroidal antiinflammatory drugs and the risk of Alzheimer's disease. *N. Engl. J. Med.* **345,** 1515–1521
13. Weggen, S., Eriksen, J. L., Sagi, S. A., Pietrzik, C. U., Ozols, V., Fauq, A., Golde, T. E., and Koo, E. H. (2003) Evidence that nonsteroidal anti-inflammatory drugs decrease amyloid β 42 production by direct modulation of γ-secretase activity. *J. Biol. Chem.* **278,** 31831–31837
14. Eriksen, J. L., Sagi, S. A., Smith, T. E., Weggen, S., Das, P., McLendon, D. C., Ozols, V. V., Jessing, K. W., Zavitz, K. H., Koo, E. H., and Golde, T. E. (2003) NSAIDs and enantiomers of flurbiprofen target γ-secretase and lower Aβ 42 *in vivo*. *J. Clin. Invest.* **112,** 440–449
15. Takahashi, Y., Hayashi, I., Tominari, Y., Rikimaru, K., Morohashi, Y., Kan, T., Natsugari, H., Fukuyama, T., Tomita, T., and Iwatsubo, T. (2003) Sulindac sulfide is a noncompetitive γ-secretase inhibitor that preferentially reduces Aβ 42 generation. *J. Biol. Chem.* **278,** 18664–18670
16. Wanngren, J., Ottervald, J., Parpal, S., Portelius, E., Strömberg, K., Borgegård, T., Klintenberg, R., Juréus, A., Blomqvist, J., Blennow, K., Zetterberg, H., Lundkvist, J., Rosqvist, S., and Karlström, H. (2012) Second generation γ-secretase modulators exhibit different modulation of Notch β and Aβ production. *J. Biol. Chem.* **287,** 32640–32650
17. Nadezhdin, K. D., Bocharova, O. V., Bocharov, E. V., and Arseniev, A. S. (2012) Dimeric structure of transmembrane domain of amyloid precursor protein in micellar environment. *FEBS Lett.* **586,** 1687–1692
18. Chen, W., Gamache, E., Rosenman, D. J., Xie, J., Lopez, M. M., Li, Y. M., and Wang, C. (2014) Familial Alzheimer's mutations within APPTM increase Aβ42 production by enhancing accessibility of ϵ-cleavage site. *Nat. Commun.* **5,** 3037
19. Barrett, P. J., Song, Y., Van Horn, W. D., Hustedt, E. J., Schafer, J. M., Hadziselimovic, A., Beel, A. J., and Sanders, C. R. (2012) The amyloid precursor protein has a flexible transmembrane domain and binds cholesterol. *Science* **336,** 1168–1171
20. Manrique-Moreno, M., Moreno, M. M., Garidel, P., Suwalsky, M., Howe, J., and Brandenburg, K. (2009) The membrane-activity of Ibuprofen, Diclofenac, and Naproxen: a physico-chemical study with lecithin phospholipids. *Biochim. Biophys. Acta* **1788,** 1296–1303
21. Hüsch, J., Dutagaci, B., Glaubitz, C., Geppert, T., Schneider, G., Harms, M., Müller-Goymann, C. C., Fink, L., Schmidt, M. U., Setzer, C., Zirkel, J., Rebmann, H., Schubert-Zsilavecz, M., and Abdel-Tawab, M. (2011) Structural properties of so-called NSAID-phospholipid-complexes. *Eur. J. Pharm. Sci.* **44,** 103–116
22. Lichtenberger, L. M., Zhou, Y., Jayaraman, V., Doyen, J. R., O'Neil, R. G., Dial, E. J., Volk, D. E., Gorenstein, D. G., Boggara, M. B., and Krishnamoorti, R. (2012) Insight into NSAID-induced membrane alterations, pathogenesis and therapeutics: characterization of interaction of NSAIDs with phosphatidylcholine. *Biochim. Biophys. Acta* **1821,** 994–1002
23. Kukar, T. L., Ladd, T. B., Bann, M. A., Fraering, P. C., Narlawar, R., Maharvi, G. M., Healy, B., Chapman, R., Welzel, A. T., Price, R. W., Moore, B., Rangachari, V., Cusack, B., Eriksen, J., Jansen-West, K., Verbeeck, C., Yager, D., Eckman, C., Ye, W., Sagi, S., Cottrell, B. A., Torpey, J., Rosenberry, T. L., Fauq, A., Wolfe, M. S., Schmidt, B., Walsh, D. M., Koo, E. H., and Golde, T. E. (2008) Substrate-targeting γ-secretase modulators. *Nature* **453,** 925–929
24. Botev, A., Munter, L. M., Wenzel, R., Richter, L., Althoff, V., Ismer, J., Gerling, U., Weise, C., Koksch, B., Hildebrand, P. W., Bittl, R., and Multhaup, G. (2011) The amyloid precursor protein C-terminal fragment C100 occurs in monomeric and dimeric stable conformations and binds γ-secretase modulators. *Biochemistry* **50,** 828–835
25. Richter, L., Munter, L. M., Ness, J., Hildebrand, P. W., Dasari, M., Unterreitmeier, S., Bulic, B., Beyermann, M., Gust, R., Reif, B., Weggen, S., Langosch, D., and Multhaup, G. (2010) Amyloid β 42 peptide (Aβ42)-lowering compounds directly bind to Aβ and interfere with amyloid precursor protein (APP) transmembrane dimerization. *Proc. Natl. Acad. Sci. U.S.A.* **107,** 14597–14602
26. Khalifa, N. B., Van Hees, J., Tasiaux, B., Huysseune, S., Smith, S. O., Constantinescu, S. N., Octave, J. N., and Kienlen-Campard, P. (2010) What is the role of amyloid precursor protein dimerization? *Cell Adh. Migr.* **4,** 268–272
27. Beel, A. J., Barrett, P., Schnier, P. D., Hitchcock, S. A., Bagal, D., Sanders, C. R., and Jordan, J. B. (2009) Nonspecificity of binding of γ-secretase modulators to the amyloid precursor protein. *Biochemistry* **48,** 11837–11839
28. Barrett, P. J., Sanders, C. R., Kaufman, S. A., Michelsen, K., and Jordan, J. B. (2011) NSAID-based γ-secretase modulators do not bind to the amyloid-β polypeptide. *Biochemistry* **50,** 10328–10342
29. Hirohata, M., Ono, K., Naiki, H., and Yamada, M. (2005) Non-steroidal anti-inflammatory drugs have anti-amyloidogenic effects for Alzheimer's β-amyloid fibrils *in vitro*. *Neuropharmacology* **49,** 1088–1099
30. Yesuvadian, R., Krishnamoorthy, J., Ramamoorthy, A., and Bhunia, A. (2014) Potent γ-secretase inhibitors/modulators interact with amyloid-β fibrils but do not inhibit fibrillation: a high-resolution NMR study. *Biochem. Biophys. Res. Commun.* **447,** 590–595
31. Prade, E., Lopez del Amo, J.-M., and Reif, B. (2014) *Advances in Biological Solid-State NMR: Proteins and Membrane-Active Peptides* (Separovic, F., and Naito, A., eds), pp. 533–555, The Royal Society of Chemistry, Cambridge, UK
32. Choi, J. S., Braymer, J. J., Nanga, R. P., Ramamoorthy, A., and Lim, M. H. (2010) Design of small molecules that target metal-Aβ species and regulate metal-induced Aβ aggregation and neurotoxicity. *Proc. Natl. Acad. Sci. U.S.A.* **107,** 21990–21995
33. Rezaei-Ghaleh, N., Andreetto, E., Yan, L. M., Kapurniotu, A., and Zweckstetter, M. (2011) Interaction between amyloid β peptide and an aggregation blocker peptide mimicking islet amyloid polypeptide. *PLoS ONE* **6,** e20289
34. Yoo, S. I., Yang, M., Brender, J. R., Subramanian, V., Sun, K., Joo, N. E., Jeong, S. H., Ramamoorthy, A., and Kotov, N. A. (2011) Inhibition of amyloid peptide fibrillation by inorganic nanoparticles: functional similarities with proteins. *Angew. Chem. Int. Ed. Engl.* **50,** 5110–5115
35. Vivekanandan, S., Brender, J. R., Lee, S. Y., and Ramamoorthy, A. (2011) A partially folded structure of amyloid-β(1–40) in an aqueous environment. *Biochem. Biophys. Res. Commun.* **411,** 312–316
36. Ramamoorthy, A., and Lim, M. H. (2013) Structural characterization and inhibition of toxic amyloid-β oligomeric intermediates. *Biophys. J.* **105,** 287–288
37. Lopez del Amo, J. M., Fink, U., Dasari, M., Grelle, G., Wanker, E. E., Bieschke, J., and Reif, B. (2012) Structural properties of EGCG-induced, nontoxic Alzheimer's disease Aβ oligomers. *J. Mol. Biol.* **421,** 517–524
38. Masuda, Y., Fukuchi, M., Yatagawa, T., Tada, M., Takeda, K., Irie, K., Akagi, K., Monobe, Y., Imazawa, T., and Takegoshi, K. (2011) Solid-state NMR analysis of interaction sites of curcumin and 42-residue amyloid β-protein fibrils. *Bioorg. Med. Chem.* **19,** 5967–5974
39. Mithu, V. S., Sarkar, B., Bhowmik, D., Das, A. K., Chandrakesan, M., Maiti, S., and Madhu, P. K. (2014) Curcumin alters the salt bridge-containing turn region in amyloid β(1–42) aggregates. *J. Biol. Chem.* **289,** 11122–11131
40. Sato, M., Murakami, K., Uno, M., Nakagawa, Y., Katayama, S., Akagi, K., Masuda, Y., Takegoshi, K., and Irie, K. (2013) Site-specific inhibitory mechanism for amyloid β42 aggregation by catechol-type flavonoids targeting the Lys residues. *J. Biol. Chem.* **288,** 23212–23224
41. Schütz, A. K., Soragni, A., Hornemann, S., Aguzzi, A., Ernst, M., Böckmann, A., and Meier, B. H. (2011) The amyloid-Congo red interface at atomic resolution. *Angew. Chem. Int. Ed. Engl.* **50,** 5956–5960
42. Dasari, M., Espargaro, A., Sabate, R., Lopez del Amo, J. M., Fink, U., Grelle, G., Bieschke, J., Ventura, S., and Reif, B. (2011) Bacterial inclusion bodies of Alzheimer's disease β-amyloid peptides can be employed to study native-like aggregation intermediate states. *ChemBioChem* **12,** 407–423
43. Walsh, D. M., Thulin, E., Minogue, A. M., Gustavsson, N., Pang, E., Teplow, D. B., and Linse, S. (2009) A facile method for expression and purification of the Alzheimer's disease-associated amyloid β-peptide.

FEBS J. **276,** 1266–1281
44. Lopez del Amo, J. M., Schmidt, M., Fink, U., Dasari, M., Fändrich, M., and Reif, B. (2012) An asymmetric dimer as the basic subunit in Alzheimer's disease amyloid β fibrils. *Angew. Chem. Int. Ed. Engl.* **51,** 6136–6139
45. Bloembergen, N. (1949) On the interaction of nuclear spins in a crystalline lattice. *Physica* **15,** 386–426
46. Szeverenyi, N. M., Sullivan, M. J., and Maciel, G. E. (1982) Observation of spin exchange by two-dimensional Fourier transform 13C cross polarization-magic-angle spinning. *J. Magn. Reson.* **47,** 462–475
47. Hing, A. W., Vega, S., and Schaefer, J. (1992) Transferred-echo double-resonance NMR. *J. Magn. Reson.* **96,** 205–209
48. Hing, A. W., Vega, S., and Schaefer, J. (1993) Measurement of heteronuclear dipolar coupling by transferred-echo double-resonance NMR. *J. Magn. Reson.* **103,** 151–162
49. Castellani, F., van Rossum, B. J., Diehl, A., Rehbein, K., and Oschkinat, H. (2003) Determination of solid-state NMR structures of proteins by means of three-dimensional ^{15}N-^{13}C-^{13}C dipolar correlation spectroscopy and chemical shift analysis. *Biochemistry* **42,** 11476–11483
50. Takegoshi, K., Nakamura, S., and Terao, T. (2001) ^{13}C-^{1}H dipolar-assisted rotational resonance in magic-angle spinning NMR. *Chem. Phys. Lett.* **344,** 631–637
51. Gullion, T., and Schaefer, J. (1989) Rotational-echo double-resonance NMR. *J. Magn. Reson.* **81,** 196–200
52. Jaroniec, C. P., Filip, C., and Griffin, R. G. (2002) 3D TEDOR NMR experiments for the simultaneous measurement of multiple carbon-nitrogen distances in uniformly ^{13}C,^{15}N-labeled solids. *J. Am. Chem. Soc.* **124,** 10728–10742
53. Petkova, A. T., Yau, W. M., and Tycko, R. (2006) Experimental constraints on quaternary structure in Alzheimer's β-amyloid fibrils. *Biochemistry* **45,** 498–512
54. Paravastu, A. K., Leapman, R. D., Yau, W. M., and Tycko, R. (2008) Molecular structural basis for polymorphism in Alzheimer's β-amyloid fibrils. *Proc. Natl. Acad. Sci. U.S.A.* **105,** 18349–18354
55. Goede, A., Preissner, R., and Frömmel, C. (1997) Voronoi cell: new method for allocation of space among atoms: elimination of avoidable errors in calculation of atomic volume and density. *J. Comput. Chem.* **18,** 1113–1123
56. Rother, K., Hildebrand, P. W., Goede, A., Gruening, B., and Preissner, R. (2009) Voronoia: analyzing packing in protein structures. *Nucleic Acids Res.* **37,** D393–395
57. Tsai, J., and Gerstein, M. (2002) Calculations of protein volumes: sensitivity analysis and parameter database. *Bioinformatics* **18,** 985–995
58. Delaunay, B. N. (1934) Sur la sphère vide. *B. Acad. Sci. USSR* **7,** 793–800
59. Zhang, L., and Hermans, J. (1996) Hydrophilicity of cavities in proteins. *Proteins* **24,** 433–438
60. Sherman, W., Day, T., Jacobson, M. P., Friesner, R. A., and Farid, R. (2006) Novel procedure for modeling ligand/receptor induced fit effects. *J. Med. Chem.* **49,** 534–553
61. Sherman, W., Beard, H. S., and Farid, R. (2006) Use of an induced fit receptor structure in virtual screening. *Chem. Biol. Drug Des.* **67,** 83–84
62. Schrödinger Release 2014-1: Maestro, version 9.7, Schrödinger, LLC, New York, NY, 2014
63. Friesner, R. A., Banks, J. L., Murphy, R. B., Halgren, T. A., Klicic, J. J., Mainz, D. T., Repasky, M. P., Knoll, E. H., Shelley, M., Perry, J. K., Shaw, D. E., Francis, P., and Shenkin, P. S. (2004) Glide: a new approach for rapid, accurate docking and scoring: 1: method and assessment of docking accuracy. *J. Med. Chem.* **47,** 1739–1749
64. Lu, J. X., Qiang, W., Yau, W. M., Schwieters, C. D., Meredith, S. C., and Tycko, R. (2013) Molecular structure of β-amyloid fibrils in Alzheimer's disease brain tissue. *Cell* **154,** 1257–1268
65. Petkova, A. T., Leapman, R. D., Guo, Z., Yau, W. M., Mattson, M. P., and Tycko, R. (2005) Self-propagating, molecular-level polymorphism in Alzheimer's β-amyloid fibrils. *Science* **307,** 262–265
66. Niu, Z., Zhao, W., Zhang, Z., Xiao, F., Tang, X., and Yang, J. (2014) The molecular structure of Alzheimer β-amyloid fibrils formed in the presence of phospholipid vesicles. *Angew. Chem. Int. Ed. Engl.* **53,** 9294–9297
67. Bertini, I., Gonnelli, L., Luchinat, C., Mao, J., and Nesi, A. (2011) A new structural model of Aβ40 fibrils. *J. Am. Chem. Soc.* **133,** 16013–16022
68. Petkova, A. T., Ishii, Y., Balbach, J. J., Antzutkin, O. N., Leapman, R. D., Delaglio, F., and Tycko, R. (2002) A structural model for Alzheimer's β-amyloid fibrils based on experimental constraints from solid state NMR. *Proc. Natl. Acad. Sci. U.S.A.* **99,** 16742–16747
69. Shen, Y., Delaglio, F., Cornilescu, G., and Bax, A. (2009) TALOS+: a hybrid method for predicting protein backbone torsion angles from NMR chemical shifts. *J. Biomol. NMR* **44,** 213–223
70. Tycko, R. (2006) Molecular structure of amyloid fibrils: insights from solid-state NMR. *Q. Rev. Biophys.* **39,** 1–55
71. Chimon, S., Shaibat, M. A., Jones, C. R., Calero, D. C., Aizezi, B., and Ishii, Y. (2007) Evidence of fibril-like β-sheet structures in a neurotoxic amyloid intermediate of Alzheimer's β-amyloid. *Nat. Struct. Mol. Biol.* **14,** 1157–1164
72. Ahmed, M., Davis, J., Aucoin, D., Sato, T., Ahuja, S., Aimoto, S., Elliott, J. I., Van Nostrand, W. E., and Smith, S. O. (2010) Structural conversion of neurotoxic amyloid-β(1–42) oligomers to fibrils. *Nat. Struct. Mol. Biol.* **17,** 561–567
73. Rauk, A., Armstrong, D. A., and Fairlie, D. P. (2000) Is oxidative damage by β-amyloid and prion peptides mediated by hydrogen atom transfer from glycine α-carbon to methionine sulfur within β-sheets? *J. Am. Chem. Soc.* **122,** 9761–9767
74. Rauk, A., and Armstrong, D. A. (2000) Influence of β-sheet structure on the susceptibility of proteins to backbone oxidative damage: preference for αc-centered radical formation at glycine residues of antiparallel β-sheets. *J. Am. Chem. Soc.* **122,** 4185–4192
75. Harmeier, A., Wozny, C., Rost, B. R., Munter, L. M., Hua, H., Georgiev, O., Beyermann, M., Hildebrand, P. W., Weise, C., Schaffner, W., Schmitz, D., and Multhaup, G. (2009) Role of amyloid-β glycine 33 in oligomerization, toxicity, and neuronal plasticity. *J. Neurosci.* **29,** 7582–7590
76. Kanski, J., Varadarajan, S., Aksenova, M., and Butterfield, D. A. (2002) Role of glycine-33 and methionine-35 in Alzheimer's amyloid β-peptide 1–42-associated oxidative stress and neurotoxicity. *Biochim. Biophys. Acta* **1586,** 190–198
77. Brunelle, P., and Rauk, A. (2002) The radical model of Alzheimer's disease: specific recognition of Gly29 and Gly33 by Met35 in a β-sheet model of Aβ: an ONIOM study. *J. Alzheimers Dis.* **4,** 283–289
78. Hou, L., Kang, I., Marchant, R. E., and Zagorski, M. G. (2002) Methionine 35 oxidation reduces fibril assembly of the amyloid aβ-(1–42) peptide of Alzheimer's disease. *J. Biol. Chem.* **277,** 40173–40176
79. McGovern, S. L., Caselli, E., Grigorieff, N., and Shoichet, B. K. (2002) A common mechanism underlying promiscuous inhibitors from virtual and high-throughput screening. *J. Med. Chem.* **45,** 1712–1722
80. Coan, K. E., and Shoichet, B. K. (2008) Stoichiometry and physical chemistry of promiscuous aggregate-based inhibitors. *J. Am. Chem. Soc.* **130,** 9606–9612
81. Hagerman, A. E., and Butler, L. G. (1981) The specificity of proanthocyanidin-protein interactions. *J. Biol. Chem.* **256,** 4494–4497
82. Feng, B. Y., Toyama, B. H., Wille, H., Colby, D. W., Collins, S. R., May, B. C., Prusiner, S. B., Weissman, J., and Shoichet, B. K. (2008) Small-molecule aggregates inhibit amyloid polymerization. *Nat. Chem. Biol.* **4,** 197–199
83. Ono, K., Li, L., Takamura, Y., Yoshiike, Y., Zhu, L., Han, F., Mao, X., Ikeda, T., Takasaki, J., Nishijo, H., Takashima, A., Teplow, D. B., Zagorski, M. G., and Yamada, M. (2012) Phenolic compounds prevent amyloid β-protein oligomerization and synaptic dysfunction by site-specific binding. *J. Biol. Chem.* **287,** 14631–14643